Supplementary information

Development of a novel mouse glioma model using lentiviral vectors

Tomotoshi Marumoto, Ayumu Tashiro, Dinorah Friedmann-Morvinski, Miriam Scadeng, Yasushi Soda, Fred H. Gage and Inder M. Verma

a

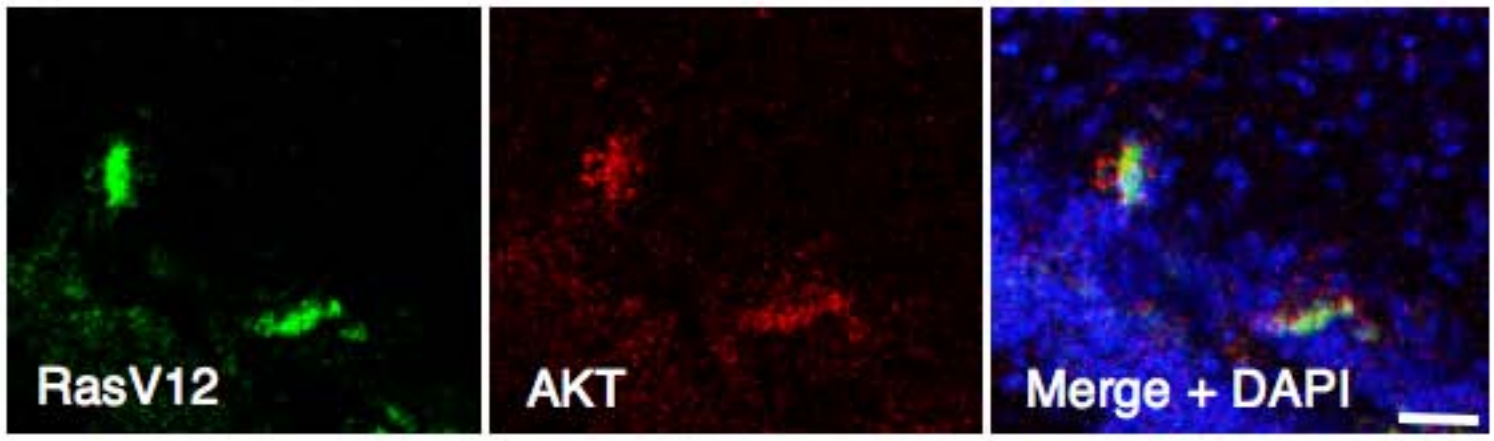

b

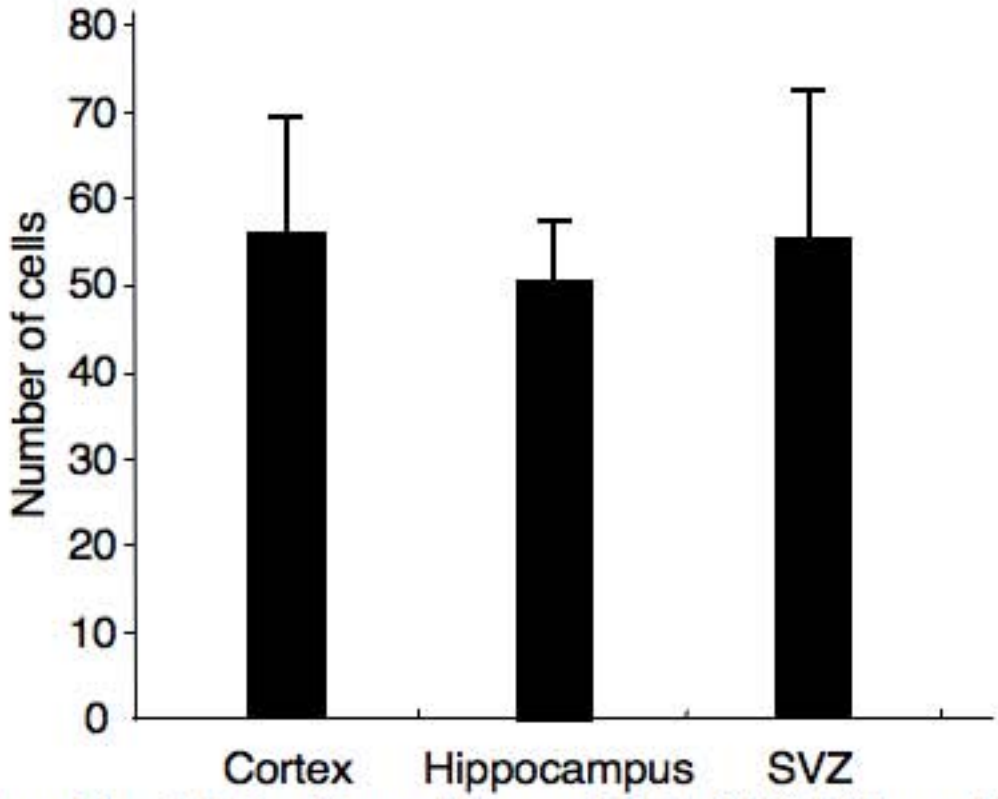

Supplementary Fig. 1 Injection of Tomo H-RasV12 LVs and Tomo AKT LVs into GFAP-Cre mouse brain. (a) Both H-RasV12 and AKT were expressed from the same cell *in vivo*. Tomo Flag H-RasV12 LVs and Tomo HA AKT LVs were injected into cortex, hippocampus and SVZ in GFAP-Cre mice at a time. Seven days after the infection, the brains were fixed and stained with Flag-specific antibody (green, left panel) and HA-specific antibody (red, middle panel). Merged image with DAPI staining (blue, nucleus) is shown in the right panel. White bar indicates 50 μm. (**b**) The number of GFAP$^+$ cells infected with both H-Ras and AKT in different locations were calculated. The results for each location were obtained from the injections into three GFAP-Cre mice with Tomo LVs. error bars, s.d.

Nature Medicine: doi:10.1038/nm.1863

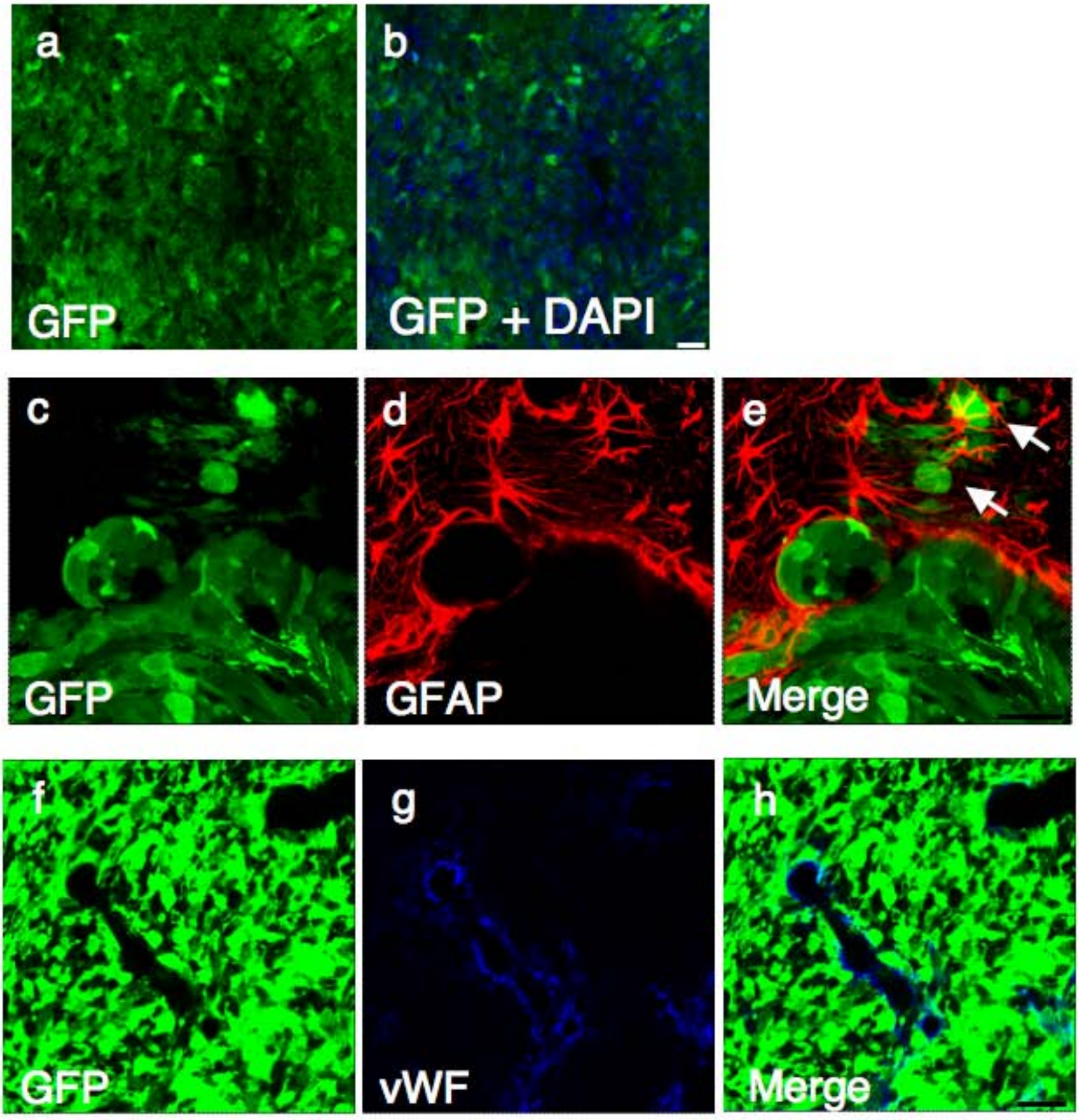

Supplementary Fig. 2 Characterization of tumors induced by combined activaton of H-Ras and AKT. (a–b) High magnification images of the tumor arose from hippocampus in GFAP-Cre mouse. GFP$^+$ tumor cells are shown in (**a**). A merged image with DAPI is shown in (**b**). (**c–e**) Representative images of the GFP$^+$/GFAP$^-$ tumor cells showing an infiltrative characteristic. GFP$^+$ tumor cells (green) arose from GFAP-Cre *Tp53*$^{+/-}$ mouse are shown in (**c**). Normal GFAP$^+$ astrocytes (red) are shown in (**d**). A merged image of (**c**) and (**d**) is shown in (**e**). (**f–h**) Sections from the tumor induced by combined activation of H-Ras and AKT in the right hippocampus of GFAP-Cre *Tp53*$^{+/-}$ mice were stained with the antibodies to GFP (**f**, green) and vWF (**g**, blue). A merged image of (**f**) and (**g**) is shown in (**h**). Note that the vessels positive for CD31/vWF in the tumor were abundant (panels **f–h** and **Fig. 4g**). White arrows in (**e**) indicate the tumor cells invading the normal tissues. Scale bars indicate 50 μm.

Nature Medicine: doi:10.1038/nm.1863

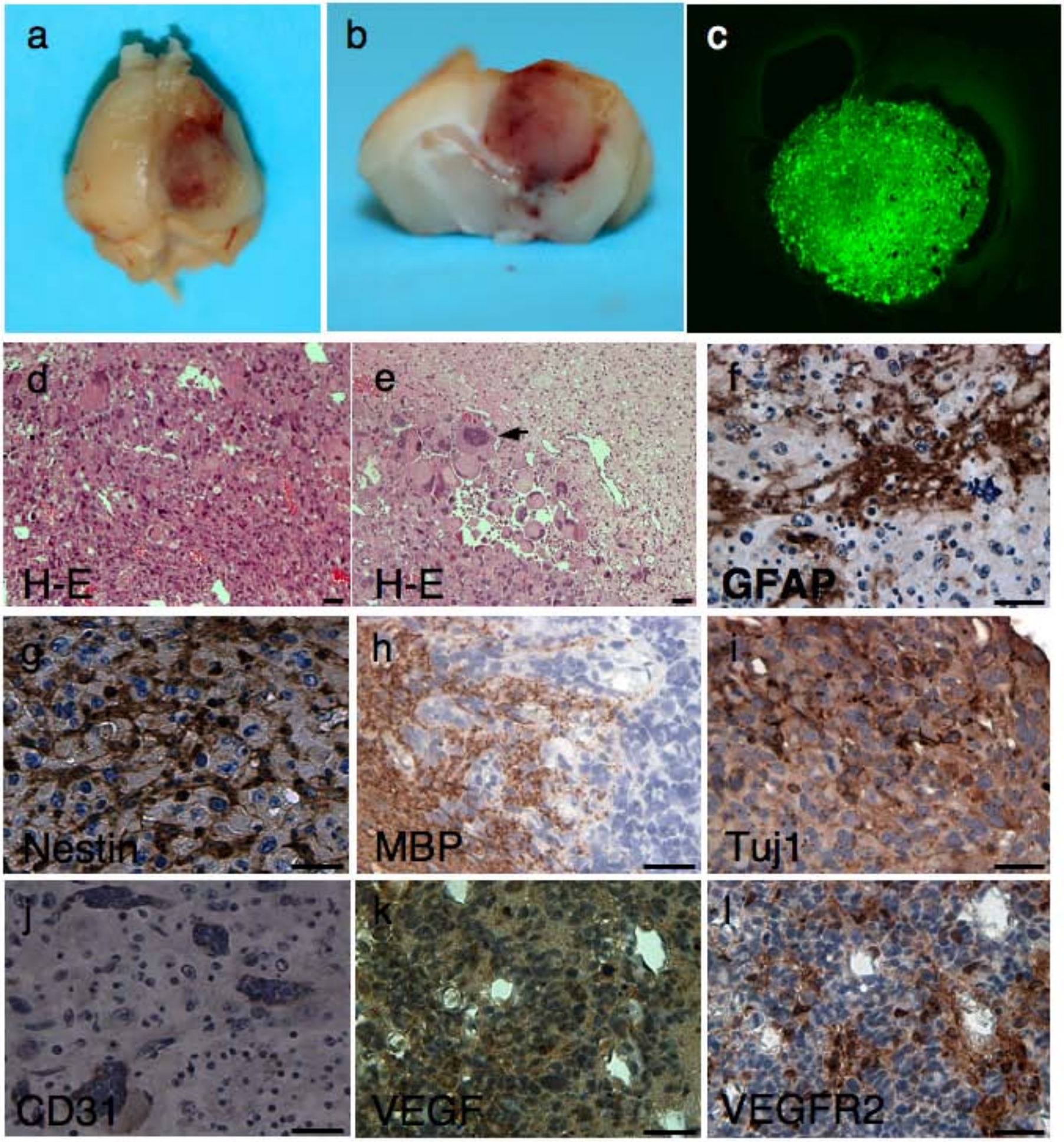

Supplementary Fig. 3 Subventricular mouse GBM induced by combined activation of H-Ras and AKT in GFAP-Cre *Tp53*$^{+/-}$ mice. (**a**) Gross appearance of the brain with GBM arose from the right SVZ. (**b**) A cross-sectional image of the tumor. (**c**) A confocal image of the tumor expressing GFP. (**d and e**) Representative images of the tumor stained with H&E are shown. A black arrow in (**e**) indicates the formation of a giant cell and nuclear pleomorphism. (**f–l**) Immunohistochemical analyses of the tumor. Sections from the tumor arose from SVZ were stained with GFAP (**f**), Nestin (**g**), MBP (**h**), Tuj1 (**i**), CD31 (**j**), VEGF (**k**) and VEGFR2 (**l**), respectively. Bars indicate 50 μm.

Nature Medicine: doi:10.1038/nm.1868

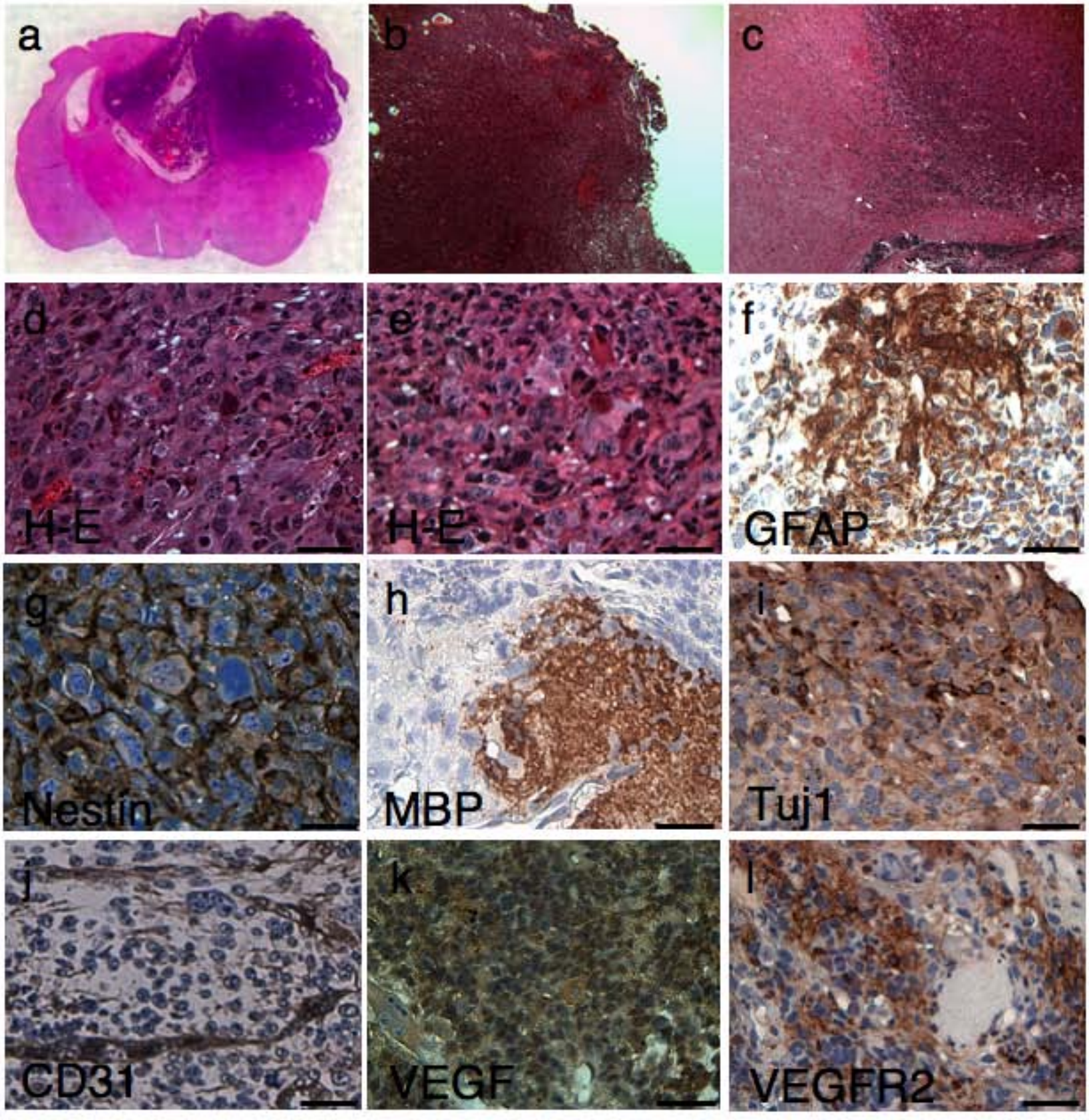

Supplementary Fig. 4 Cortex tumor induced by combined activation of H-Ras and AKT in GFAP-Cre *Tp53*$^{+/-}$ mouse. (**a–c**) A cross-sectional image is shown of a mouse GBM arose from cortex stained with H&E. High cellular density and an invasive characteristic of the tumor cells are apparent. (**d and e**) High magnification images of the tumor stained with H&E are shown. Note that nuclear pleomorphism are remarkable. (**f-l**) Immunohistochemical analyses of the tumor. Sections from the tumor arose from the cortex were stained with GFAP (**f**), Nestin (**g**), MBP (**h**), Tuj1 (**i**), CD31 (**j**), VEGF (**k**), VEGFR2 (**l**), respectively. Bars indicate 50 μm.

Nature Medicine: doi:10.1038/nm.1863

a

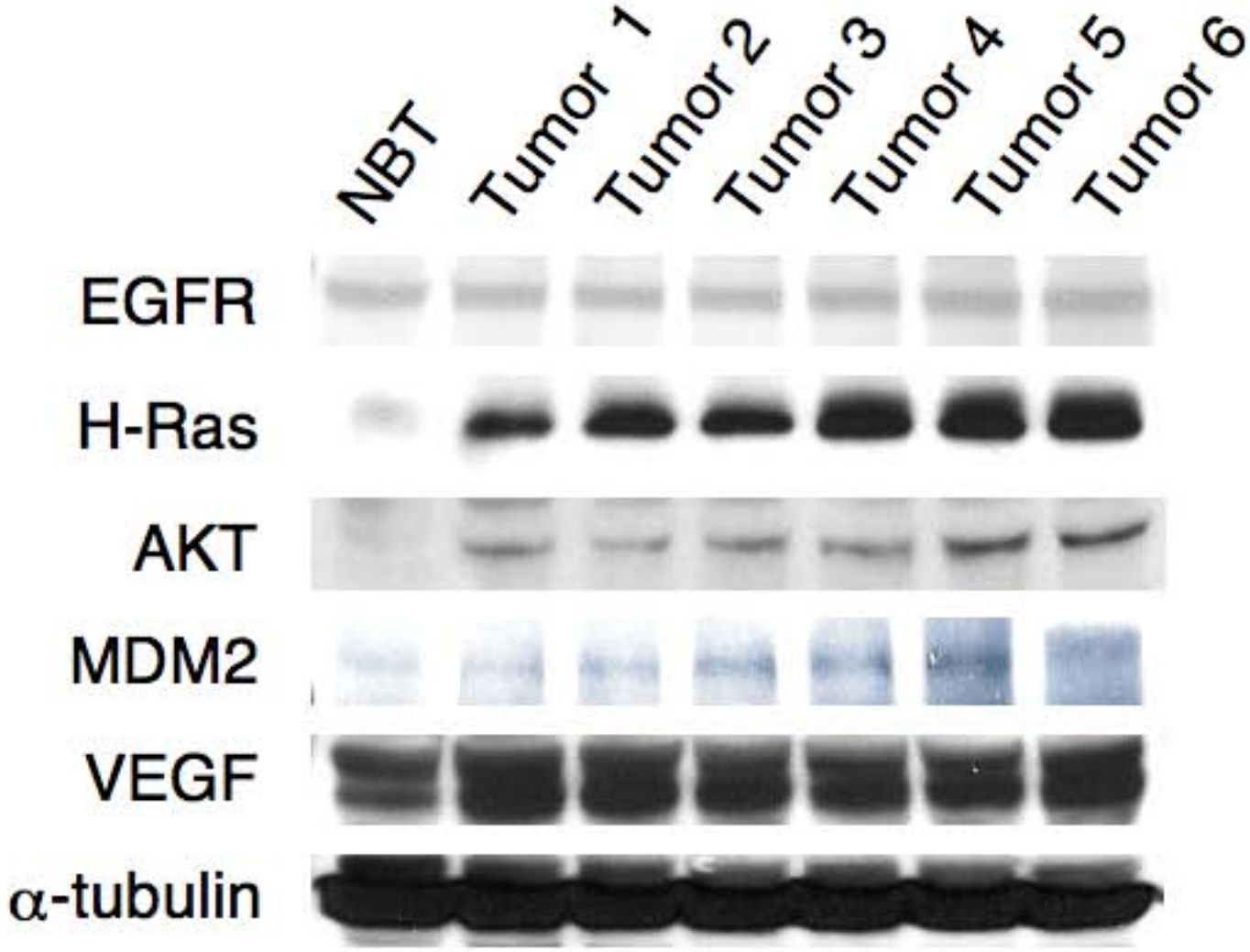

Nature Medicine: doi:10.1038/nm.1863

b

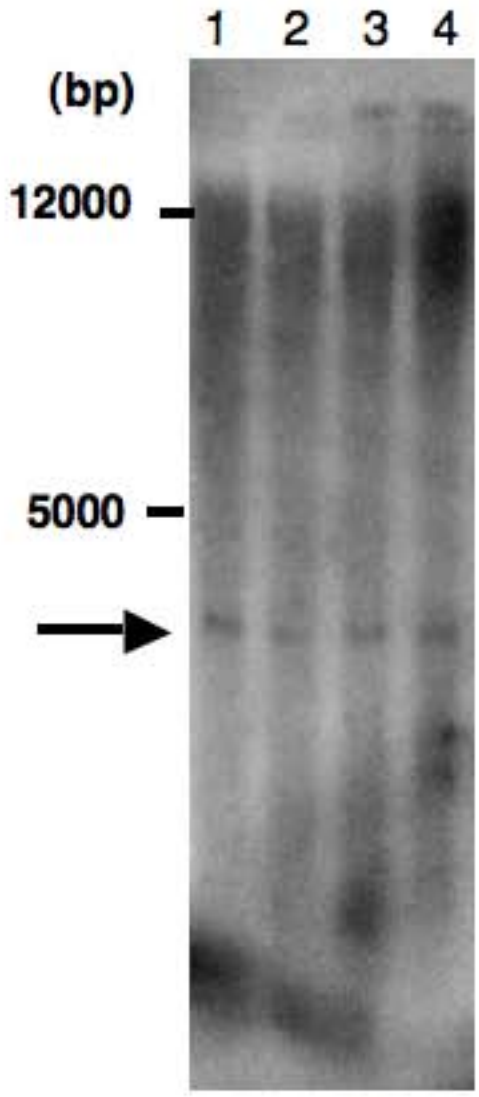

1. Normal brain tissue
2. 005 tumor cells
3. Tumor from HP
4. Tumor from SVZ

Supplementary Fig. 5 Molecular characterization of GBM induced by combined activation of H-Ras and AKT in GFAP-Cre *Tp53*$^{+/-}$ mice. (**a**) Western blotting of the mouse brain tumor tissues. Tumor samples 1–3 were prepared from the tumors induced by the combined activation of H-Ras and AKT in the right hippocampus in GFAP-Cre *Tp53*$^{+/-}$ mice. Tumor samples 4–6 were prepared from the tumors induced by combined activation of H-Ras and AKT in the right SVZ in GFAP-Cre *Tp53*$^{+/-}$ mice. α-tubulin was used as a loading control. NBT: normal brain tissue prepared from the macroscopically normal area in the brain with tumor induced by combined activation of H-Ras and AKT in the right hippocampus in GFAP-Cre *Tp53*$^{+/-}$ mice. Flag-specific antibody was used to detect H-Ras. HA-specific antibody was used to detect AKT. (**b**) Southern blotting to detect the *Cdkn2a* (encoding p16) allele in mouse GBM. A black arrow indicates the positive bands. HP: hippocampus, SVZ: subventricular zone.

Nature Medicine: doi:10.1038/nm.1863

p53

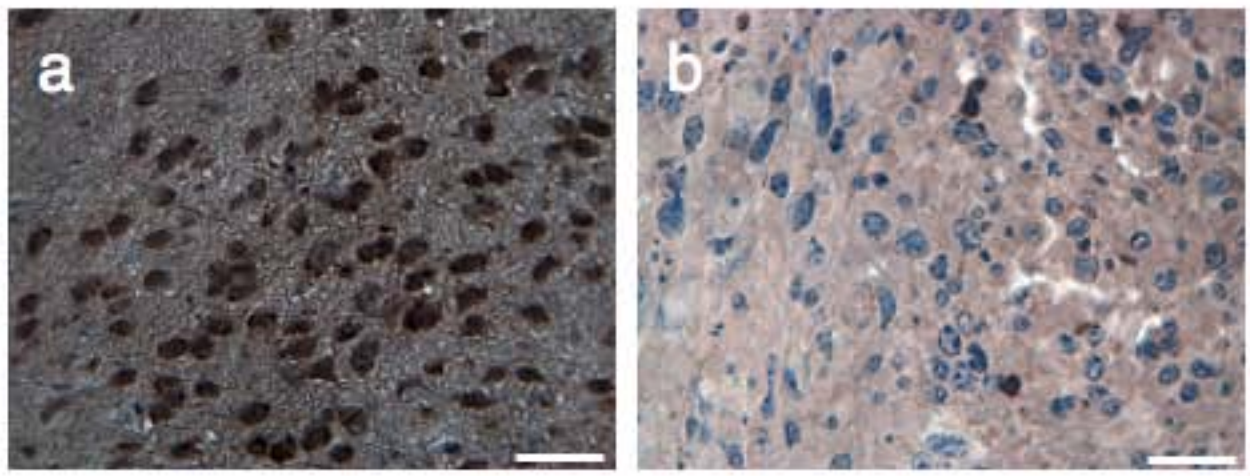

GFAP-Cre GFAP-Cre *Tp53*$^{+/-}$

GFAP-Cre GFAP-Cre GFAP-Cre *Tp53*$^{+/-}$

f

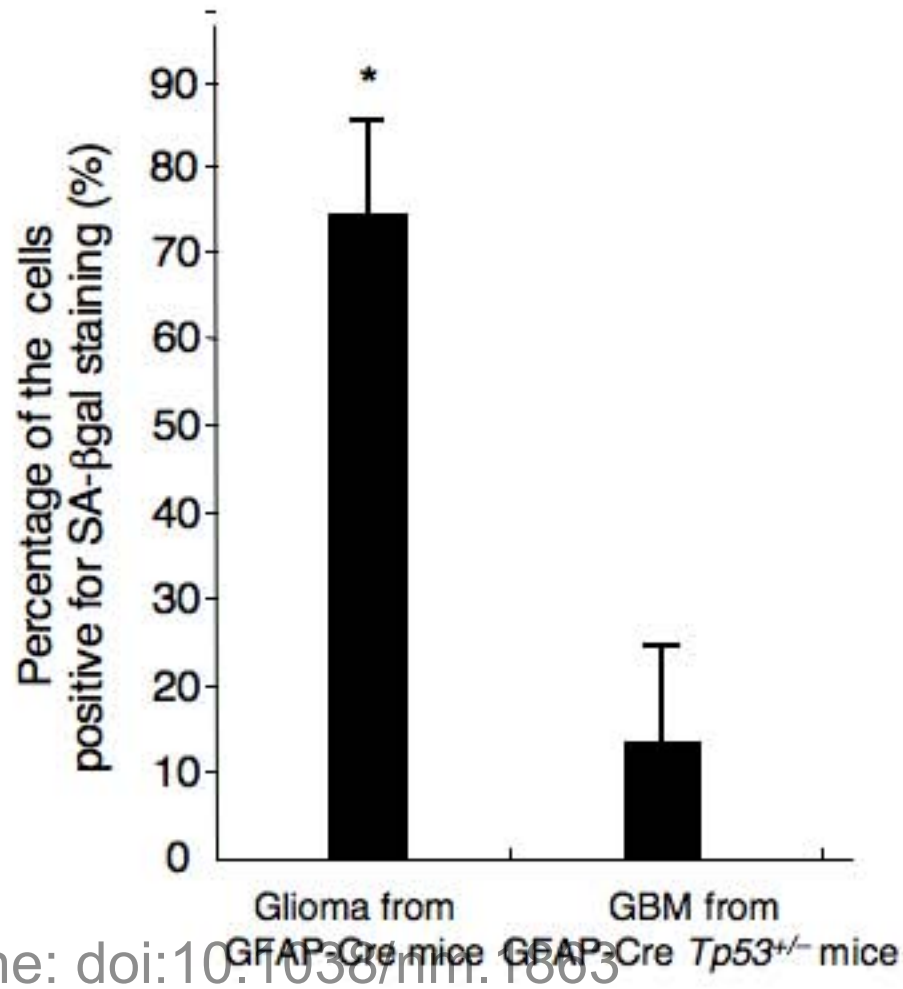

Nature Medicine: doi:10.1038/nm.1863

g

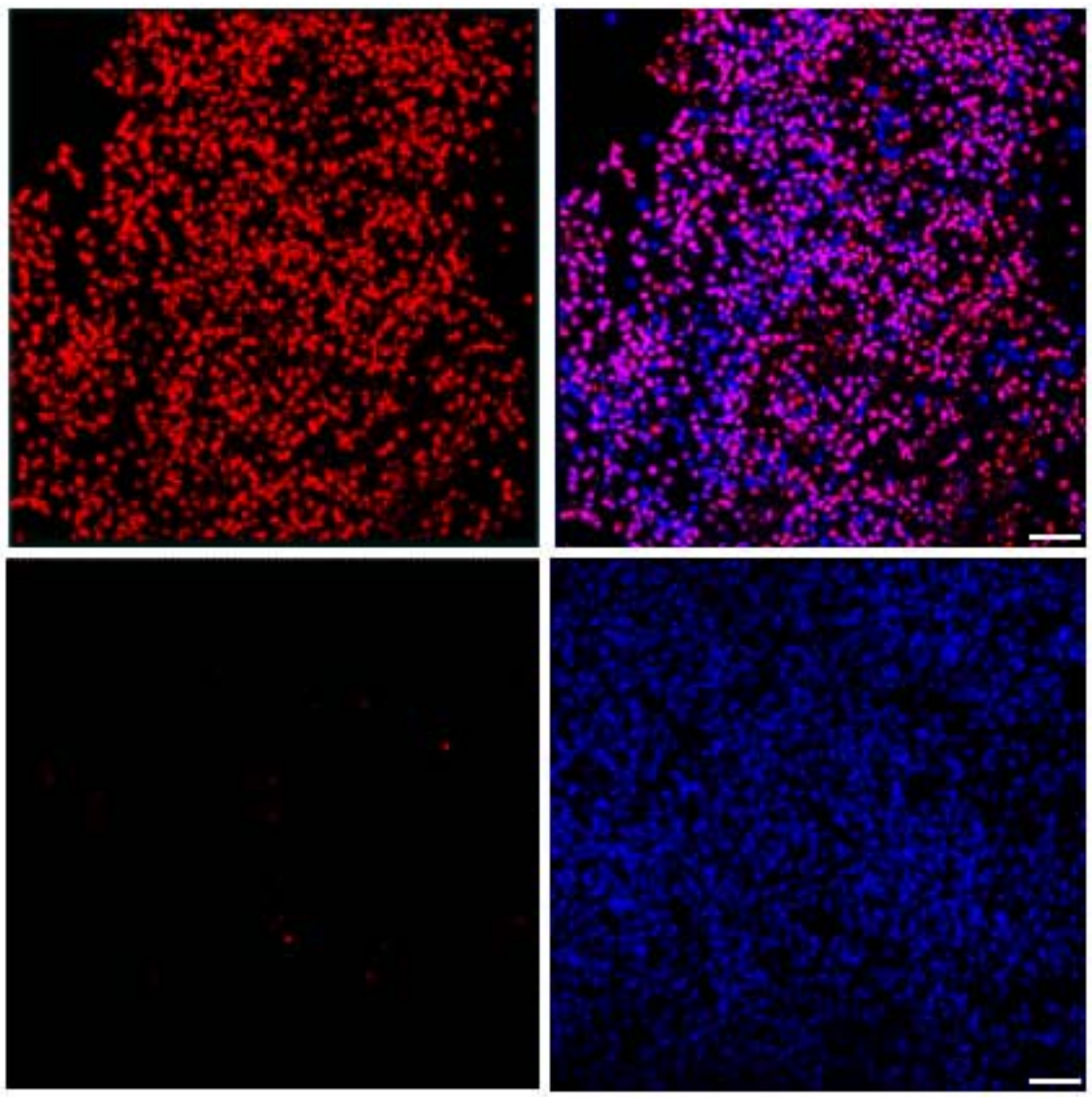

h

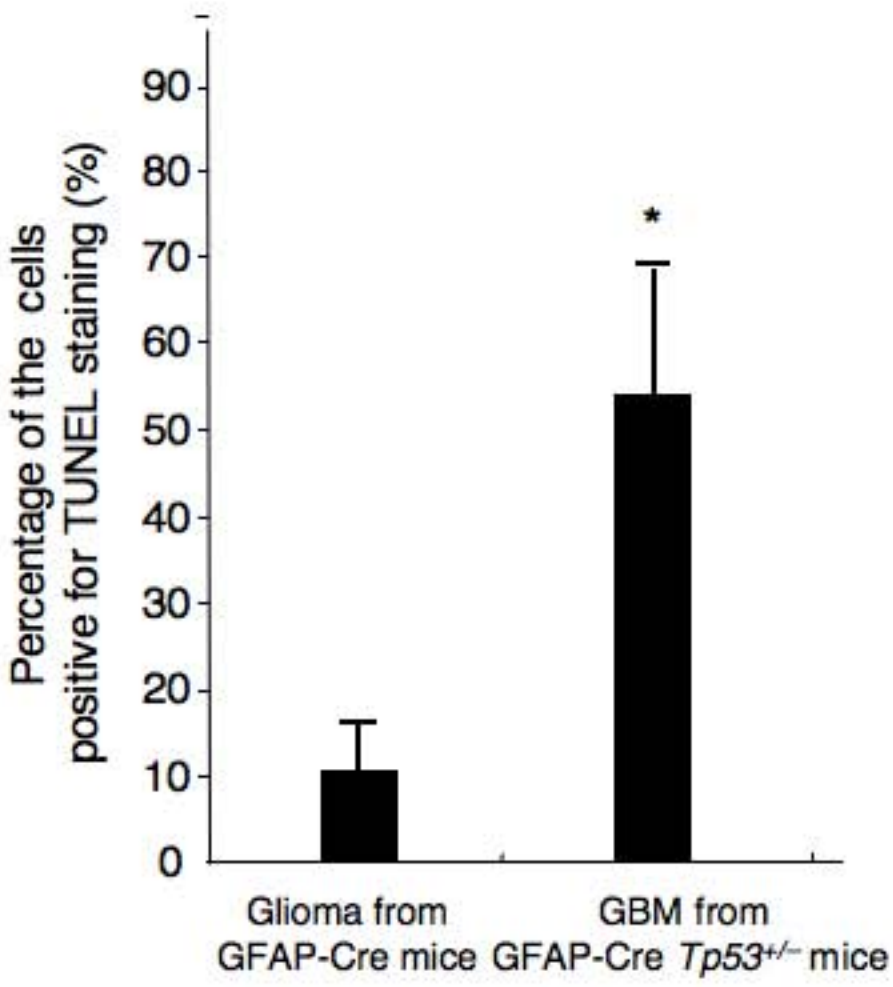

Nature Medicine: doi:10.1038/nm.1863

Supplementary Fig. 6 Senescence found in the tumor caused by combined activation of H-Ras and AKT in the hippocampus of GFAP-Cre mice. (a and b) Representative images of immunohistchemistry for p53 in the tumors derived from GFAP-Cre mice (**a**) or GFAP-Cre *Tp53*$^{+/-}$ mice (**b**). Note that expression of p53 is much higher in the tumors from GFAP-Cre mice than those from GFAP-Cre *Tp53*$^{+/-}$ mice. (**c and d**) Representative images of the tumor cells derived from the hippocampus in GFAP-Cre mice which are positive for senescence-associated β-galactosidase (SA-βgal) staining. (**e**) In contrast, few cells showed SA-βgal activity in the tumor arose from the hippocampus in GFAP-Cre *Tp53*$^{+/-}$ mice. Blue staining indicates the SA-βgal activity. (**f**) Fifteen sections of tumors found in GFAP-Cre mice and fifteen sections of the tumors from GFAP-Cre *Tp53*$^{+/-}$ mice were subjected to SA-βgal staining. At least 500 cells in each section were examined and the proportion of the cells positive for the staining were calculated, N and T in (**c**) indicate normal tissue and tumor tissue areas respectively. (**g and h**) Tumor sections were processed for TUNEL staining. The proportion of TUNEL positive cells (left panels, red) was much higher in the tumors arose from GFAP-Cre *Tp53*$^{+/-}$ mice than those from GFAP-Cre mice. Merged images with DAPI staining are shown in the right panels. Bars indicate 50 μm, $*P < 0.05$, error bars, s.d.

Nature Medicine: doi:10.1038/nm.1863

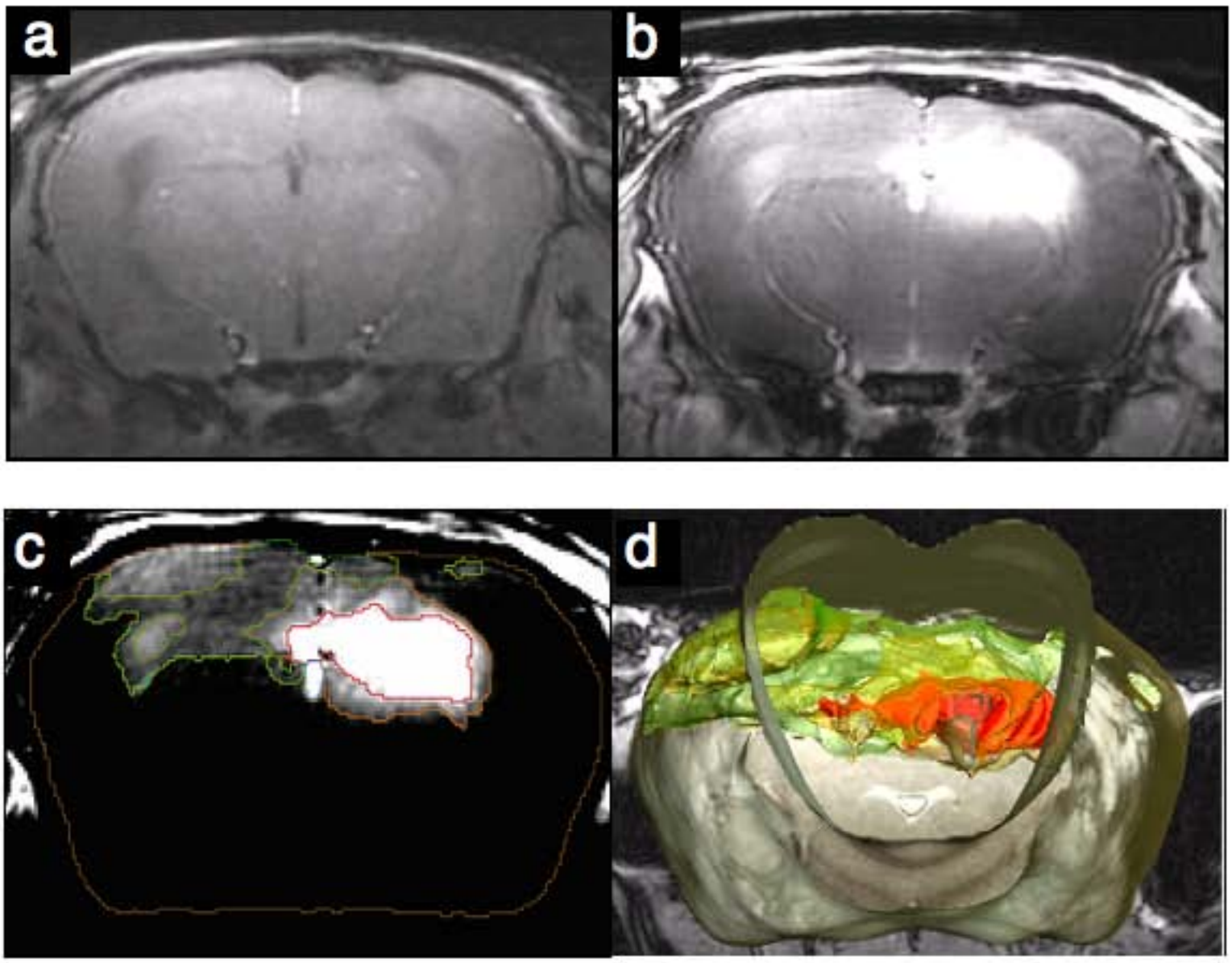

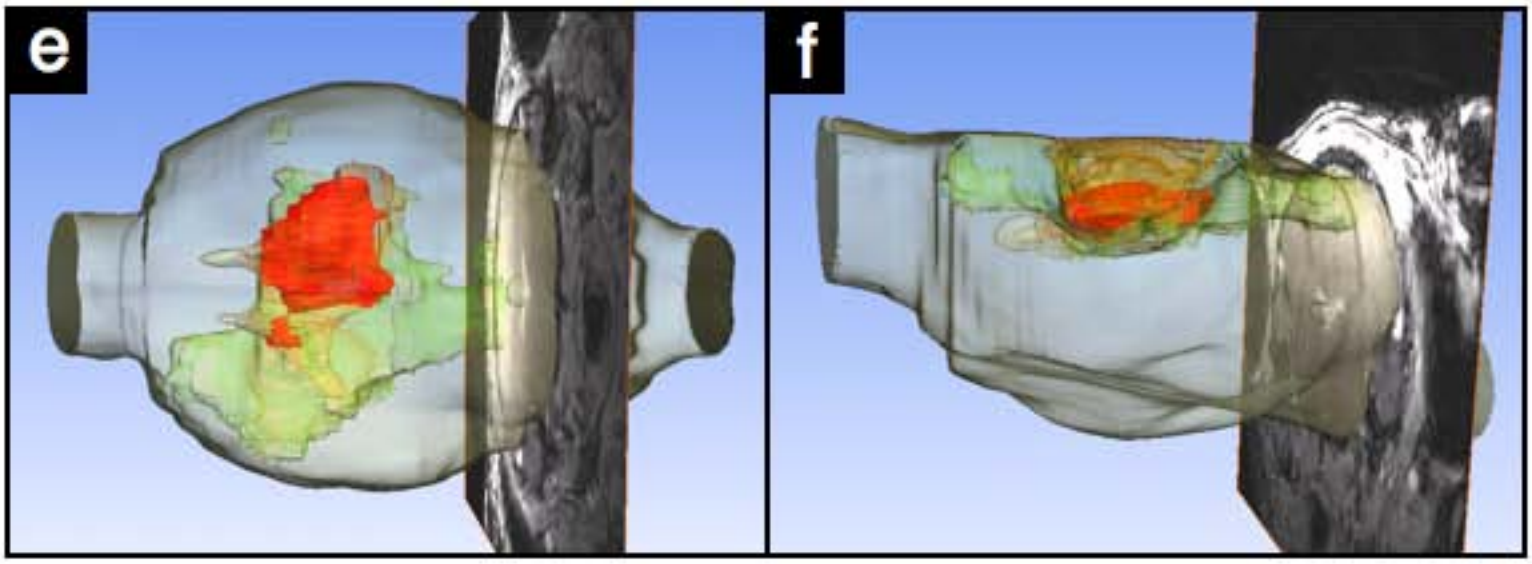

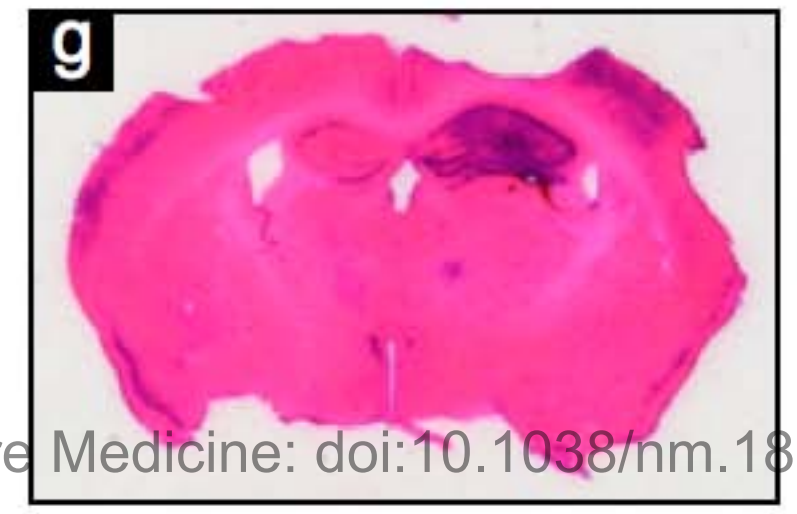

Nature Medicine: doi:10.1038/nm.1863

Supplementary Fig. 7 MRI of the tumor induced by combined activation of H-Ras and AKT in GFAP-Cre *Tp53*$^{+/-}$ mice. (**a-f**) 73 days after the injection of Tomo H-RasV12 LVs and Tomo AKT LVs into the right hippocampus, mice were processed for MRI imaging. T1 weighted 3D FSPGR images acquired pre (**a**) and post (**b**) injection of intraperitoneal gadolinium contrast agent. Areas of abnormal contrast agent uptake are enhanced and appear bright on the image. The intensity of the tissue enhancement varies within the brain tissue (**c**) the brightest area representing the most abnormal tissue and areas with less enhancement have less tumor extensive infiltrates (**d–f**) Areas of relative intensity can be color coded to produce a 3D model of the extent and distribution of the tumor cells in the brain tissue that can be viewed from multiple aspects, from front (**d**), from below (**e**) and from side (**f**). (**g**) H-E staining of the tumor imaged by MRI. The darker area indicates the tumor formation.

Nature Medicine: doi:10.1038/nm.1863

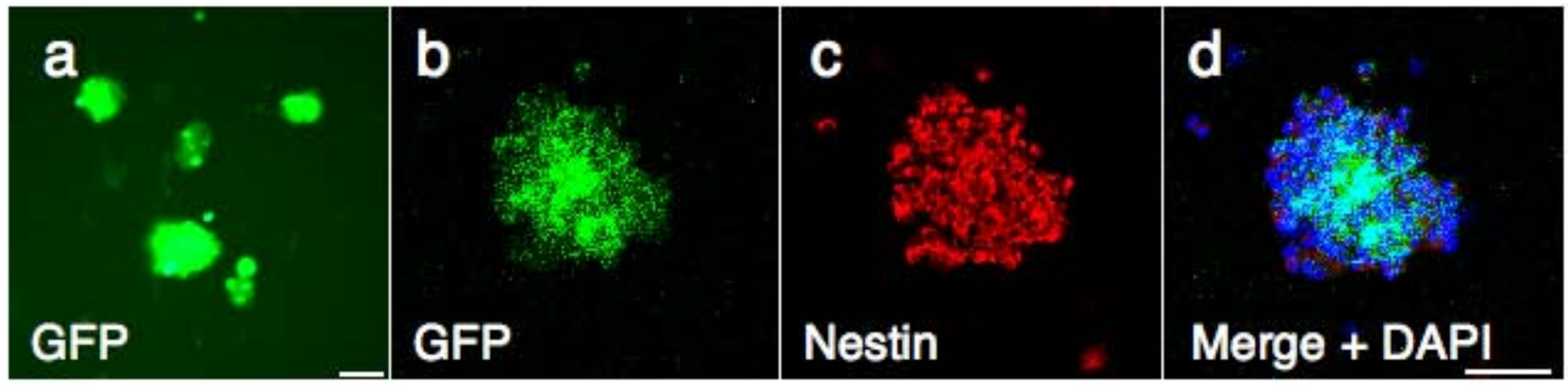

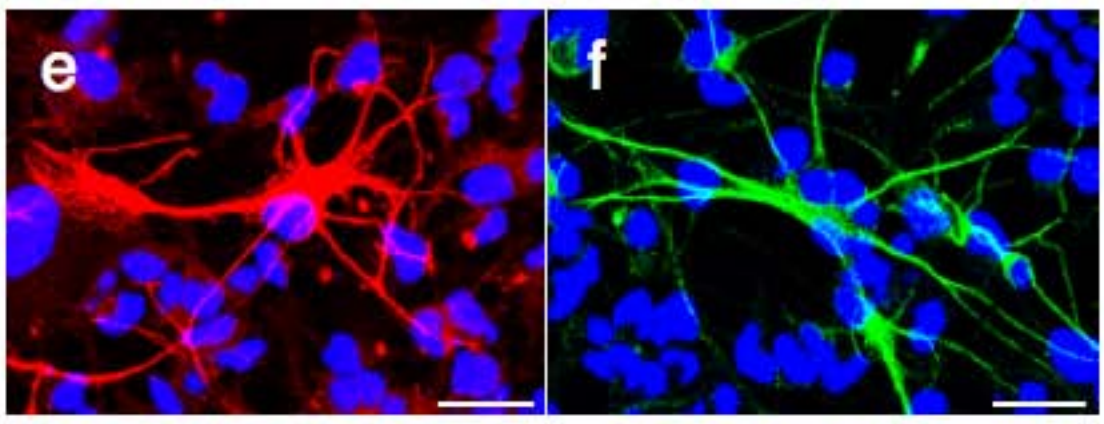

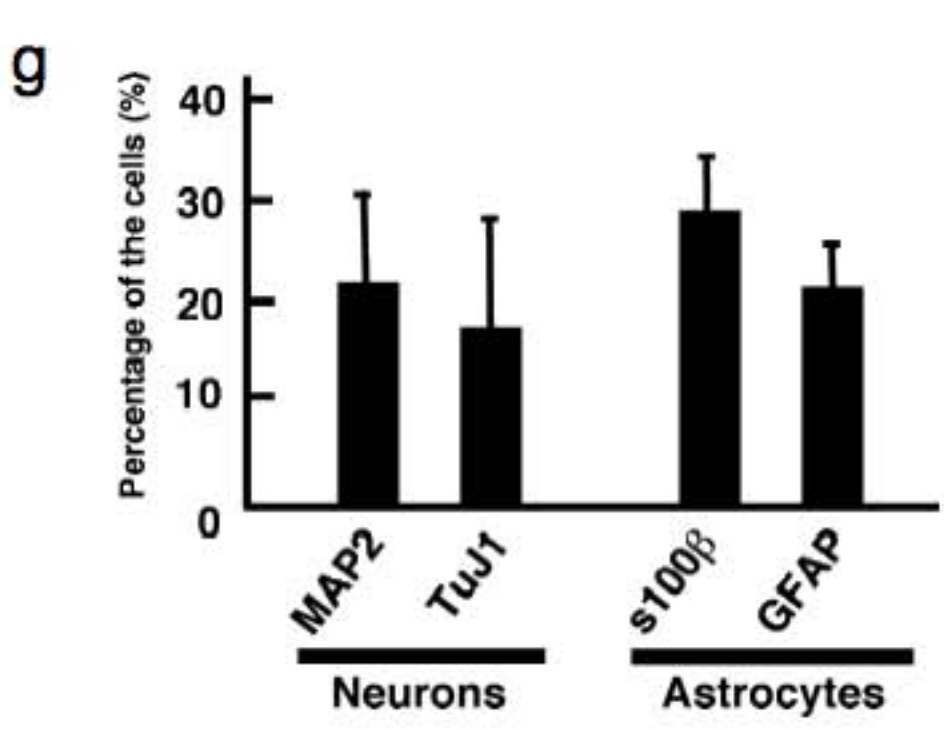

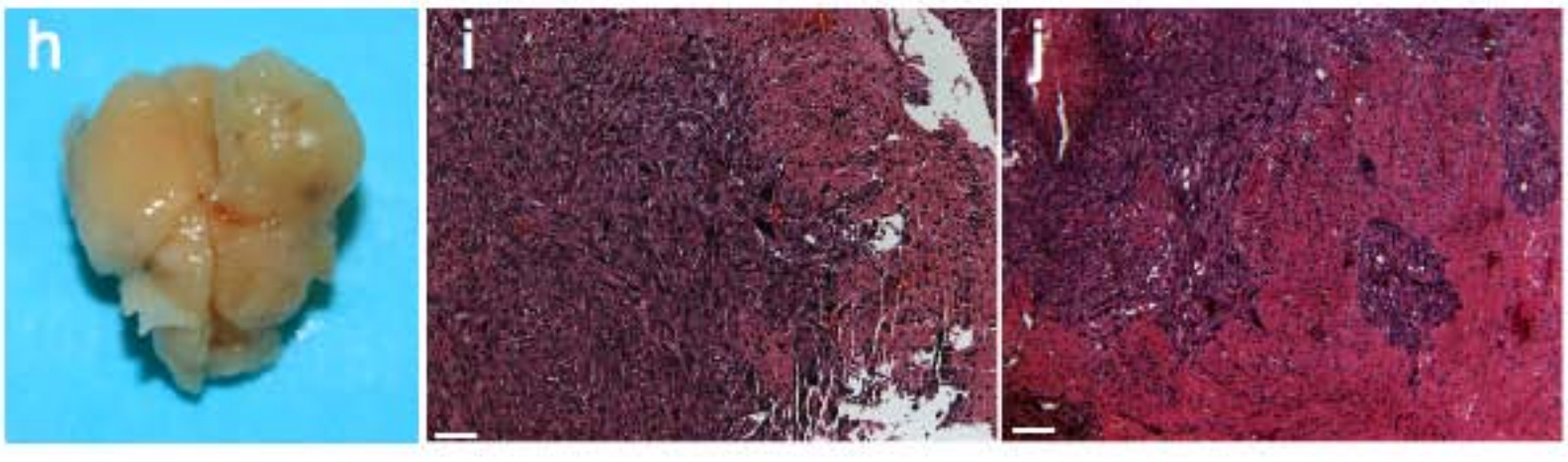

Nature Medicine: doi:10.1038/nm.1863

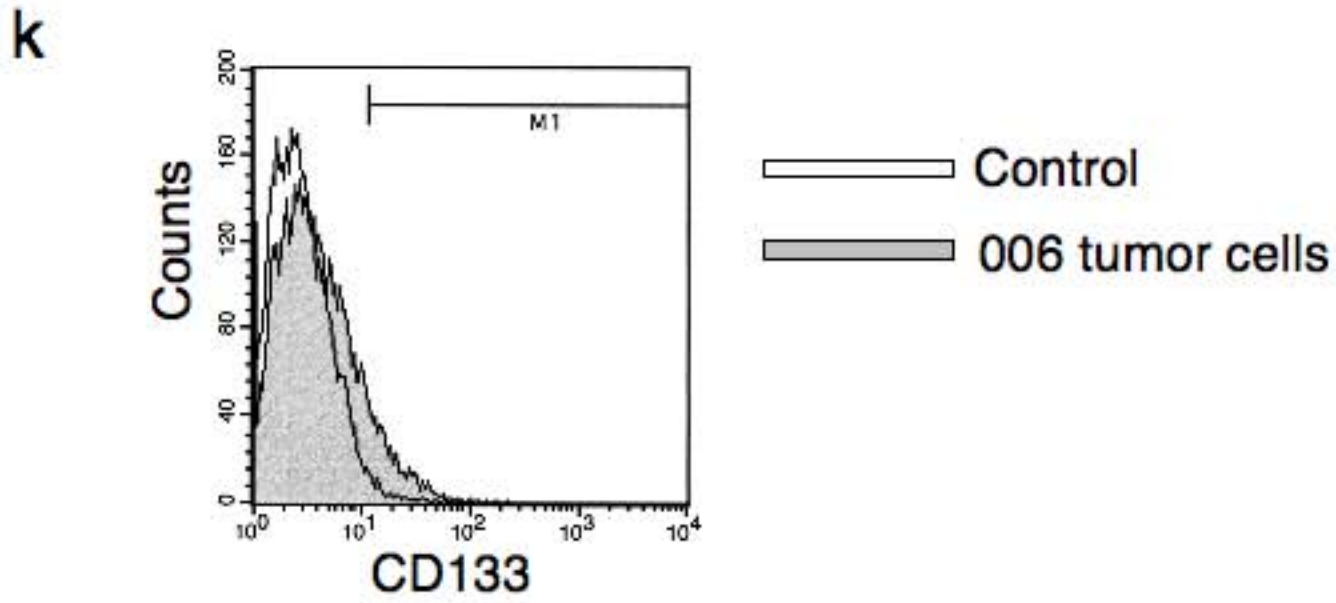

Supplementary Fig. 8 006 tumor cells showed the characteristics of the brain tumor stem/initiating cells. (**a**) A representative confocal image of GFP$^+$ tumor cells in culture. Tumor cells (006 tumor cells) from GFAP-Cre *Tp53*$^{+/-}$ mouse injected with Tomo H-RasV12 LVs and Tomo AKT LVs into the right hippocampus were able to be cultured in the medium for the neural stem cells. These cells formed neurosphere-like structures. White bar in (**a**) indicates 50 μm. (**b–d**) Most of the GFP$^+$ tumor cells (> 99%, 006 tumor cells) in culture were positive for Nestin. 006 tumor cells cultured in stem cell medium were fixed and stained with Nestin-specific antibody (**c**, red), and then images were taken by confocal microscopy. A merged image with DAPI staining was shown in (**d**). A white bar in (**d**) indicates 50 μm. (**e and f**) 006 tumor cells expressed neuronal and astrocyte markers in response to serum addition into the medium. Five days after the addition of 10% FBS into the medium cells were fixed and stained with GFAP-specific antibody (**e**, red) and Tuj1-specific antibody (**f**, green). Merged mages with DAPI are shown in (**e**) and (**f**). The proportions of cells expressed neuronal and astrocyte markers are shown in (**g**). White bars in (**e**) and (**f**) indicate 30 μm. (**h**) Injection of 006 tumor cells (1×10^2) causes the tumor formation in NOD SCID mice. The gross appearance of the brain formed tumor is shown. (**i and j**) Histological characteristics of the tumor caused by the injection of 006 tumor cells in NOD SCID mice were examined by H&E staining. Note that the tumor showed very similar characteristics to their original GBM-like tumor such as high cellular density and invasion. White bars in (**i**) and (**j**) indicate 50 μm. (**k**) About 8% of 006 tumor cells are positive for CD133. 006 tumor cells in culture were fixed and stained with CD133-specific antibody, and then they were analyzed by flow cytometry. Unstained cells were used as a control. error bars, s.d.

Nature Medicine: doi:10.1038/nm.1863

Supplementary Table 1　Summary of all the injections with Tomo lentiviral vectors

Strain	Area of injection	Oncogene	Tumor incidence
GFAP-Cre	CTX	Mock	0/10
GFAP-Cre	HP	Mock	0/10
GFAP-Cre	SVZ	Mock	0/10
GFAP-Cre	CTX	H-Ras	0/9
GFAP-Cre	HP	H-Ras	0/10
GFAP-Cre	SVZ	H-Ras	0/10
GFAP-Cre	CTX	AKT	0/8
GFAP-Cre	HP	AKT	0/10
GFAP-Cre	SVZ	AKT	0/9
GFAP-Cre	CTX	H-Ras + AKT	0/9
GFAP-Cre	HP	H-Ras + AKT	5/12
GFAP-Cre	SVZ	H-Ras + AKT	1/9
GFAP-Cre/p53$^{+/-}$	CTX	Mock	0/10
GFAP-Cre/p53$^{+/-}$	HP	Mock	0/9
GFAP-Cre/p53$^{+/-}$	SVZ	Mock	0/10
GFAP-Cre/p53$^{+/-}$	CTX	H-Ras	0/9
GFAP-Cre/p53$^{+/-}$	HP	H-Ras	6/10
GFAP-Cre/p53$^{+/-}$	SVZ	H-Ras	1/10
GFAP-Cre/p53$^{+/-}$	CTX	AKT	0/10
GFAP-Cre/p53$^{+/-}$	HP	AKT	0/10
GFAP-Cre/p53$^{+/-}$	SVZ	AKT	0/10
GFAP-Cre/p53$^{+/-}$	CTX	H-Ras + AKT	1/15
GFAP-Cre/p53$^{+/-}$	HP	H-Ras + AKT	17/17
GFAP-Cre/p53$^{+/-}$	SVZ	H-Ras + AKT	12/16

CTX: cortex, HP: hippocampus, SVZ: subventricular zone

Supplementary Table 2 Summary of histological characteristics of the gliomas caused by combined activation of H-Ras and AKT in the different locations

Strain	Area of origin	High cellular density	Pleomor-phism	Necrosis	Invasion	High vascularity	Intratumoral hemorrhage
GFAP-Cre	HP	+++	+	+	++	++	+
GFAP-Cre	HP	+++	+	+	++	++	–
GFAP-Cre	HP	+++	+	++	++	++	+
GFAP-Cre	SVZ	+++	+	+	++	++	–
GFAP-Cre/p53$^{+/-}$	HP	+++	+++	++	++	+++	+++
GFAP-Cre/p53$^{+/-}$	HP	+++	+++	++	++	+++	+++
GFAP-Cre/p53$^{+/-}$	HP	+++	+++	+	++	+++	+++
GFAP-Cre/p53$^{+/-}$	HP	+++	+++	++	++	+++	++
GFAP-Cre/p53$^{+/-}$	HP	+++	+++	++	++	+++	++
GFAP-Cre/p53$^{+/-}$	SVZ	+++	+++	++	+	+++	++
GFAP-Cre/p53$^{+/-}$	SVZ	+++	+++	++	+	+++	+
GFAP-Cre/p53$^{+/-}$	SVZ	+++	+++	+	++	+++	+
GFAP-Cre/p53$^{+/-}$	SVZ	+++	+++	++	+	+++	+
GFAP-Cre/p53$^{+/-}$	SVZ	+++	+++	++	++	+++	+
GFAP-Cre/p53$^{+/-}$	CTX	+++	+++	+	++	+++	+

CTX: cortex, HP: hippocampus, SVZ: subventricular zone, +++ : highly found, ++ : moderately found, + : weakly found. – : not found

Supplementary Table 3 Summary of antibodies used in this study

Antibody	Manufacture
Flag (M2)	Sigma Aldrich
HA	Sigma
Cre	Novagen
β-actin	Sigma
EGFR	Cell Signaling
VEGF	abcam
MDM2	abcam
α-tubulin	Sigma
GFAP	Dako
Nestin	Pharmingen
RIP	Hybridoma bank
S100β	Swant
Map2ab	Sigma
NeuN	Chemicon
Alexa 488 anti-rabbit IgG	Invitrogen
Alexa 568 anti-rabbit IgG	Invitrogen
Alexa 633 anti-rabbit IgG	Invitrogen
Alexa 568 anti-mouse IgG	Invitrogen
Alexa 633 anti-mouse IgG	Invitrogen
Alexa 568 anti-rat IgG	Invitrogen
Alexa 647 anti-rat IgG	Invitrogen
DYKDDDDK Tag	Cell Signaling
HA	Santa Cruz
Ki67	Vector
Tuj1	Covance
MBP	Serotec
CD133	eBioscience
p53	abcam